~~Multiyear~~ Two-year statistics of columnar ice production in stratiform clouds over Hyytiälä, Finland: environmental conditions and the relevance to secondary ice production

Haoran Li[1,2], Ottmar Möhler[3], Tuukka Petäjä[2], and Dmitri Moisseev[2,3]

[1]State Key Laboratory of Severe Weather, Chinese Academy of Meteorological Sciences, Beijing, China
[2]Institute for Atmospheric and Earth System Research / Physics, Faculty of Science, University of Helsinki, Finland
[3]Institute of Meteorology and Climate Research, Karlsruhe Institute of Technology, Karlsruhe, Germany
[4]Finnish Meteorological Institute, Helsinki, Finland

Correspondence: Haoran Li (haoran.li@helsinki.fi)

Abstract. Formation of ice particles in clouds at the temperatures of -10 ~~°C~~ °C or warmer was documented by using ground-based ~~remote sensing~~ radar observations. At these temperatures, the number concentration of ice nucleating particles (~~INP~~INPs) is not only expected to be small, but also this number is highly uncertain. In addition, there are a number of studies reporting that the observed number concentration of ice particles exceeds expected INP concentrations, indicating that other ice generation mechanisms, such as secondary ice production (SIP), may play an important role in such clouds. To identify ~~the~~ formation of ice crystals and report conditions in which they are generated, W-band cloud radar Doppler spectra observations collected at the Hyytiälä station for more than two years were used. Given that at these temperatures ice crystals grow mainly as columns, which have distinct linear depolarization ratio (LDR) values, spectral LDR was utilized to identify newly formed ice particles. ~~Our results indicate that that the columnar ice production took place~~ It is found that in 5 ~~to~~ $\sim$ 13 ~~%~~% of clouds, where cloud top temperatures ~~were~~ are -12 ~~C or higher~~°C or warmer, production of columnar ice is detected. For colder clouds, this percentage can be as high as 33 ~~%~~%. 40 $\sim$ 50 ~~%~~% of columnar-ice-producing events last less than 1 hour, while 5 $\sim$ 15 ~~%~~% can persist for more than 6 hours. By comparing clouds where columnar crystals ~~were produced with~~ are produced and to the ones where these crystals ~~were absent, we found that~~ are absent, the columnar-ice-producing clouds tend to have larger values of liquid water path and precipitation intensity. The columnar-ice-producing clouds were subdivided into ~~subcategories~~three categories, using the temperature difference, ΔT, between the altitudes where columns are first detected and ~~the cloud top altitude~~cloud top. The cases where ΔT is less than 2 ~~°C~~K are typically single-layer shallow clouds where needles are produced at the cloud top. In multilayered clouds ~~, where $\Delta T >$~~ where 2 ~~°C~~K $< \Delta T$, columns are produced in a layer that is seeded by ice particles falling from above. This classification allows to study potential impacts of various SIP mechanisms, such as Hallet-Mossop process or freezing breakup, on columnar ice production. To answer the question whether the observed ice particles are generated by SIP in the observed single-layer shallow clouds, ice particle number concentrations were retrieved and compared to several INP parameterizations. It was found that the ice number concentrations tend to be 1 $\sim$ 3 orders of magnitude higher than the expected INP concentrations.

1 Introduction

Ice production in mixed-phase clouds is critical for their radiative (Sun and Shine, 1994) and microphysical (Korolev et al., 2017) properties. At temperatures warmer than -38 ~~°C~~°C, ice crystals form on ice nucleating particles (INPs). In-situ measurements have revealed that the number concentration of available INPs ~~steeply~~ decreases with the increase of ambient temperature (e.g., DeMott et al., 2010; Wilson et al., 2015; DeMott et al., 2016; Petters and Wright, 2015; Schneider et al., 2020). This dependence is more or less universal~~and seems to depend only marginally on~~, but can also be affected by other factors such as the geographic location, airmass types and aerosol compositions ~~(DeMott et al., 2010; Wilson et al., 2015; DeMott et al., 2016; Petters and Wr~~ ~~.~~(e.g., DeMott et al., 2010; Niemand et al., 2012; Wilson et al., 2015; DeMott et al., 2016; Petters and Wright, 2015; McCluskey et al., 20 . In addition, it has been found that INP concentrations in high latitudes are generally lower than in mid-latitudes (e.g., DeMott et al., 2016; \ . Above -10 ~~°C~~°C, the typical concentrations of INPs are below 10 $^{-1}$ ~~per Liter (L^{-1})~~ L^{-1} and can be as low as 10^{-6} ~~L^{-1}~~ L^{-1} (Petters and Wright, 2015; Kanji et al., 2017). A number of studies, however, have reported that the ice number concentration in clouds with the top temperature warmer than -10 ~~°C~~°C can exceed the expected concentration of INPs by several orders of magnitude (e.g., Mossop, 1985; Hobbs and Rangno, 1985; Rangno and Hobbs, 2001). This discrepancy implies that numerical weather prediction models that rely solely on INP parameterizations cannot realistically represent ice number concentrations in moderately to slightly supercooled clouds. As a result, the inappropriate parameterization of ice production may lead to biased estimates of surface shortwave radiation budget (Young et al., 2019), among other things (e.g., Zhao et al., 2021; Zhao and Liu, 2021).

Several mechanisms have been proposed to explain this discrepancy, such as the enhanced contact nucleation driven by the thermophoretic force during the evaporation of liquid drops (Beard, 1992; Hobbs and Rangno, 1985), pre-activated INPs from evaporated ice particles nucleated above (Roberts and Hallett, 1968; Fridlind et al., 2007) or secondary ice production (SIP) mechanisms (see recent reviews by Field et al., 2017; Korolev and Leisner, 2020). The SIP has been studied by a number of laboratory experiments since 1940s (e.g., Findeisen and Findeisen, 1943; Dye and Hobbs, 1966; Wildeman et al., 2017). Hallett and Mossop (1974) have found that numerous ice splinters can be generated when supercooled liquid drops ~~with the diameter~~ larger than $\sim$ ~~24~~ 25 μm are collected by large ice particles within the temperature range of -8 ~~°C~~°C $\sim$ -3 ~~°C~~°C. This is referred as to Hallett–Mossop (H-M) process, the most studied and ~~the only implemented~~ ~~secondary ice production (SIP)~~ most frequently implemented SIP mechanism in numerical ~~cloud, weather, and climate models~~ ~~(Morrison et al., 2005)~~models (Field et al., 2017), despite that more parameterizations for other SIP processes are becoming available (e.g., Hoarau et al., 2018; Sullivan et al., 2018; Zhao et al., 2021). The enhanced ice number concentration can also be caused by the fragmentation of large supercooled liquid droplets (e.g., Evans and Hutchinson, 1963; Scott and Hobbs, 1977; Wildeman et al., 2017). It has been found that the secondary ice production efficiency is positively correlated with the size of liquid droplets (Lauber et al., 2018) and is enhanced in moist environment (Keinert et al., 2020). At temperatures higher than -3 ~~°C~~°C the fragmentation of drizzle is still active as shown by field observations (Lauber et al., 2021). In addition, studies using optical sensors mounted on aircrafts have reported the high concentration of ice columns within the temperature range of -10 $\sim$ -3 ~~°C~~°C (e.g., Koenig, 1963; Hobbs and Rangno, 1990; Rangno and Hobbs, 2001). Based on aircraft mea-

surements from two field campaigns, Korolev et al. (2020) have concluded that the secondary ice process is highly associated with the presence of liquid droplets and aged rimed ice in turbulent regions. Recently, Yang et al. (2020) have found that the ice concentration in tropical maritime stratiform clouds characterized by the top temperature above -8 °C is in the order of $10^{-1} \sim 10^1$ L^{-1}, which cannot be fully explained by primary ice nucleation, H-M process or droplet freezing. However, despite the advantage of offering a direct way of interpreting ice microphysics, aircraft observations are only available from a few measurement campaigns, and do not seem sufficient for a long-term assessment.

The polarimetric variables, such as differential reflectivity (Z_{dr}), specific differential phase measurements (K_{dp}) and linear depolarization ratio (LDR), observed by dual-polarization radars are sensitive to the shape of hydrometeors (Bringi and Chandrasekar, 2001) and allow the analysis of ice particles with specific habits (e.g., Matrosov et al., 2001; Hogan et al., 2002; Tyynelä and Chandrasekar, 2014; Li et al., 2018). At temperatures of -10 $\sim$ -2 °C, the depositional growth of an ice crystal is stronger at the basal faces than at the prism faces. Hence, the formation of columnar ice is preferred (Lamb and Verlinde, 2011). This distinct habit can produce high Z_{dr} and K_{dp} as observed by dual-polarization weather radars (Hogan et al., 2002; Giangrande et al., 2016; Sinclair et al., 2016). For vertically-pointing Ka- and W-band radars, ice columns usually produce LDR values as high as -15 dB, which is distinctively higher than that of most other ice particle types (Aydin and Walsh, 1999; Tyynelä et al., 2011). Oue et al. (2015); Li and Moisseev (2020); Luke et al. (2021); have shown that this strong LDR signal at the slow falling part of radar Doppler spectrum can be used to identify columnar ice crystals. In this study, this method is applied to long-term radar Doppler spectra observations for characterizing the production of columnar ice particles in stratiform clouds. Similar to (Luke et al., 2021) we show that this phenomenon is not uncommon. By comparing radar-based retrievals of ice number concentrations to INP parameterizations, one of which was derived from observations collected at our measurement site (Schneider et al., 2020), we show that the ice number concentrations tend to be $1 \sim 3$ orders of magnitude higher than the expected INP concentration. This also supports the conclusions reached by Luke et al. (2021).

The paper is organized as follows. Section 2 introduces the data used in this study. The method for identifying columnar ice particles from radar Doppler spectra is illustrated in Sect. 3. Statistical results are presented in Sect. 4. Section 5 compares the concentrations of columnar ice particles and INPs in single-layer shallow clouds. Conclusions are given in Sect. 6.

2 Data

2.1 Cloud radar observations

The measurements used in this study were collected at Station for Measuring Ecosystem - Atmosphere Relations II (Hari and Kulmala, 2005; Petäjä et al., 2016) located in Hyytiälä, Southern Finland (61.845°N, 24.287°E, 150 m above mean sea level, amsl.). Since November 2017, a 94-GHz dual-polarization frequency-modulated continuous-wave Doppler cloud radar (Küchler et al., 2017) (HYytiälä Doppler RAdar, HYDRA-W) has been operating at the station. The radar is pointing vertically and measures radar signal spectral moments, linear depolarization ratio (LDR) and dual-polarization Doppler spectra, see (Li and Moisseev, 2020) for the example of the data. The LDR decoupling is about 30 dB, so the minimum observable LDR is

90   about -30 dB. The radar operates using three chirps that define range resolution, Doppler unambiguous velocity and spectral resolution at three range intervals. Between 102 m and 996 m, the range resolution is 25.5 m, Doppler unambiguous velocity is 10.24 ~~$m\,s^{-1}$~~ $\mathrm{m\,s^{-1}}$ and the Doppler spectral resolution is 0.02 ~~$m\,s^{-1}$~~ $\mathrm{m\,s^{-1}}$. Between 996 and 3577 m, these values are 25.5 m, 5.12 ~~$m\,s^{-1}$~~ $\mathrm{m\,s^{-1}}$ and 0.02 ~~$m\,s^{-1}$~~ $\mathrm{m\,s^{-1}}$, respectively. For ranges above 3577 m, they are 34 m, 5.12 ~~$m\,s^{-1}$~~ $\mathrm{m\,s^{-1}}$ and 0.02 ~~$m\,s^{-1}$~~ $\mathrm{m\,s^{-1}}$, respectively. In this study, HYDRA-W observations recorded between February 2018 and April 2020 were

95   utilized (Moisseev, 2020).

To remove noise from Doppler spectra observations, the spectral lines with the signal-to-noise ratio less than 5 dB were filtered out. Since both co-polar and cross-polar observations were used, i.e. to compute spectral LDR, this filtering could result in complete removal of the cross-polar signal, the power of which is typically $15 \sim 30$ dB lower than that of the co-polar signal (Bringi and Chandrasekar, 2001; Moisseev et al., 2002). In such cases, no LDR values were computed.

100   The antenna diameter of HYDRA-W is 0.5 m which translates to the Fraunhofer far-field distance of 157 m (Sekelsky, 2002; Falconi et al., 2018) and antenna beam width of 0.56 ~~$^{\circ}$~~$^{\circ}$. Therefore, the lowest radar range bin, which is not affected by the near-field effect, is 179 m (the fourth range bin). Data recorded at distance in the radar far-field were used in this study, therefore limiting the lowest altitude to 179 m where observations were taken.

In addition to the active remote sensing system, HYDRA-W is capable of estimating the liquid water path (LWP) by using

105   the 89 GHz passive microwave channel observations. The brightness temperature at this band is regularly calibrated using liquid nitrogen. The site specific relation between the measured 89 GHz brightness temperature and LWP was derived by the radar manufacturer using radio-sounding and reanalysis data.

2.2 Model temperature and humidity profiles

To obtain information on atmospheric state during the cloud observations, ~~the output from~~ forecasts of the Deutscher Wetterdienst

110   (DWD) operational global Icosahedral Nonhydrostatic (ICON) model (Zängl et al., 2015) ~~was~~ were used. The ~~ICON model~~ microphysics scheme in ICON is inherited from the COSMO model (Seifert, 2008). The ICON model output is provided over all Aerosol, Clouds and Trace Gases Research Infrastructure (ACTRIS) cloud profiling stations (available at http://~~develoudnet~~cloudnet.fmi. The model data has hourly temporal resolution ~~, and the~~ with the horizontal resolution of 13 km (Prill et al., 2019; Reinert et al., 2020). The height resolution decreases with the increase of altitude, for example the height resolution is 0.16 km at the altitude of 1

115   km. Its atmospheric products, such as temperature, relative humidity (RH) and pressure, over Hyytiälä were interpolated into the temporal and spatial resolutions of HYDRA-W (CLU, 2021).

3 Methods

The mean Doppler velocity (MDV) of hydrometeors observed by a vertically pointing radar is the combination of particle terminal fall velocities and the vertical component of air motion. While Doppler velocity alone could be used to identify certain

120   types of particles (Mosimann, 1995; Kneifel and Moisseev, 2020), there are associated limitations. These limitations include, uncertainties in hydrometeor classification due to similarities of terminal fall velocities of different particles (Locatelli and

Hobbs, 1974; Barthazy and Schefold, 2006; Li et al., 2020), presence of a mixture of ice particle populations within the radar volume (Zawadzki et al., 2001; Kalesse and Luke, 2019; Li and Moisseev, 2020) and impact of air motion on the observed MDV (Protat and Williams, 2011). By using radar Doppler spectra, instead of MDV, contributions from different particle

125 populations can be separated (e.g., Zawadzki et al., 2001; Kalesse and Luke, 2019; Radenz et al., 2019; Li and Moisseev, 2020; Luke et al., 2021). In radar Doppler spectral power observations, the presence of multiple populations of hydrometeors, such as the co-existence of supercooled liquid water and ice (e.g., Zawadzki et al., 2001; Shupe et al., 2004; Luke et al., 2010; Kalesse et al., 2016; Li and Moisseev, 2019), a mixture of different ice types (e.g., Zawadzki et al., 2001; Kalesse and Luke, 2019; Radenz et al., 2019; Li and Moisseev, 2020), could manifest as multiple spectral peaks. Even in such cases, however,

130 classification of these particles can be ambiguous.

To further improve the hydrometeor identification, dual-polarization radar observations can be used. For slant measurements the spectral differential reflectivity has been found to be useful (Spek et al., 2008). Because hydrometeors typically do not have a preferred azimuth orientation, the differential reflectivity is not very useful for the classification purposes at vertical incidence. Nonetheless, LDR can be used to identify prolate particles (Myagkov et al., 2016a, b), such as ice columns (Oue et al., 2015).

135 At the elevation angle of 90°, columnar ice particles can produce LDR signals as high as -16 ∼ -13 dB (Oue et al., 2015), while other ice particles may produce values smaller than -20 dB (e.g., Tyynelä et al., 2011). Furthermore, given the relatively small fall velocities of newly produced columns, in regions where they coexist with other ice particles they usually populate the slow falling part of the Doppler spectrum. Therefore, the slow falling part characterized by high spectral LDR (∼ -15 dB) in the Doppler spectrum indicates presence of columnar ice particles ~~(Oue et al., 2015)~~(Oue et al., 2015; Radenz et al., 2019).

140 Figure 1 shows an example of observed spectral power and LDR. Two distinct populations of ice particles can be clearly identified from Fig. 1 (a), and the slower falling one corresponds to ice columns as indicated by the high spectral LDR (Fig. 1b). The observed spectral power and LDR at 1.124 km (black dot dashed lines) are shown in Fig. 1 (c). Three distinct peaks can be identified from the spectral power, and the slower falling ice columns are well characterized by the spectral LDR exceeding -18 dB. In contrast, the spectral LDR of faster falling ice is around -25 dB which mainly depends on the cross-coupling between

145 the polarization channels (Moisseev et al., 2002) and can be much higher than the LDR signal of larger aggregates (Tyynelä et al., 2011). Interestingly, supercooled liquid water seems also present, as indicated by the well defined spectral peak at around 0 ~~$m\,s^{-1}$~~ $m\,s^{-1}$ (Zawadzki et al., 2001; Shupe et al., 2004; Luke et al., 2010; Kalesse et al., 2016; Li and Moisseev, 2019). It appears that this liquid layer extends from ∼ 0.9 km to ∼ 1.3 km (Fig. 1a). The potential mechanisms of producing these ice columns will be discussed in more detailed in following sections.

150 Given the spectral characteristics of ice columns as discussed above, the following criteria were set to identify ice columns in clouds:

- Within the slowest 1 ~~$m\,s^{-1}$~~ $m\,s^{-1}$ of the Doppler spectrum at least 3 spectral bins exceed the LDR of -18 dB.

- The temperature of the radar range bin is between -10 ~~°C~~°C and 0 ~~°C~~°C.

The observed radar Doppler spectrum is not only dependent on the scattering properties of hydrometeors in the radar volume,

155 but also is affected by the turbulent broadening (Kollias et al., 2011; Tridon and Battaglia, 2015). For example, the air at around
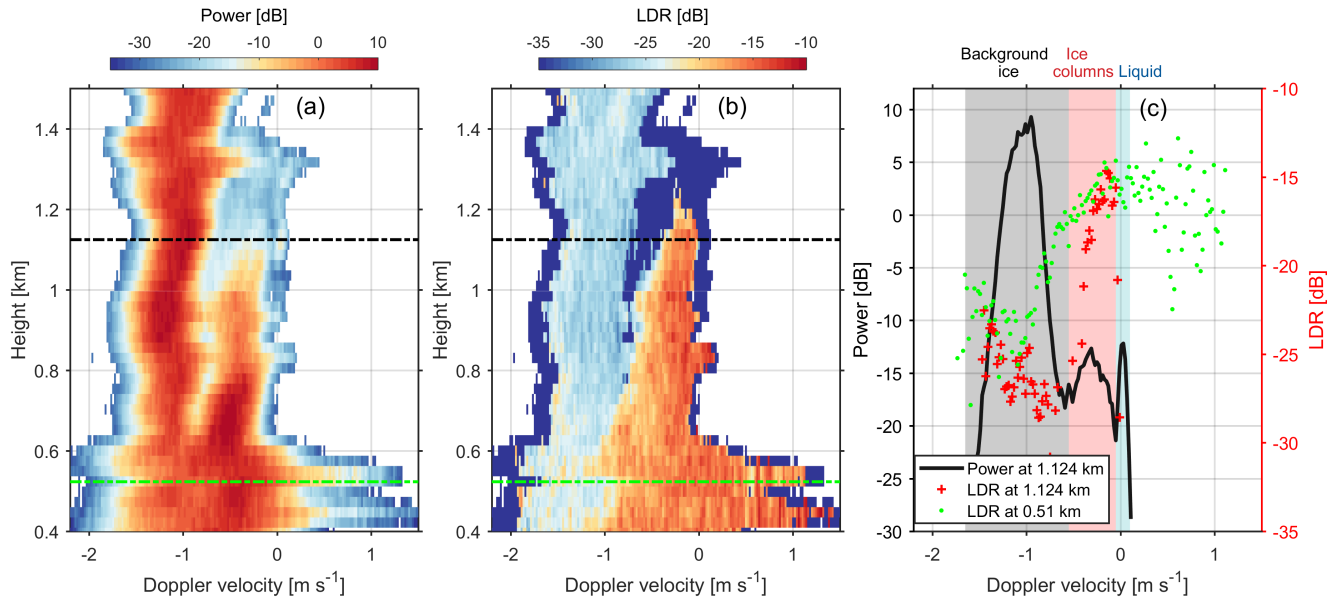
Figure 1. HYDRA-W Doppler spectral (a) power and (b) LDR at 2nd February 2018 07:56:38 UTC. (c) spectral power (black line) and LDR (red crosses) at 1.124 km as marked by the black dot dashed lines in (a) and (b), and LDR (~~blue~~ green dots) at 0.51 km as marked by the ~~blue~~ green dot dashed lines in (a) and (b). The gray, red and blue shading areas in (c) indicate background ice falling from above, newly-formed ice columns and supercooled liquid, respectively, at 1.124 km. Negative velocity indicates downward motion downwards.

0.51 km seems rather turbulent as indicated by the spectral power (~~blue~~ green dashed line in Fig. 1a). However, it appears that this issue does not significantly affect the results of columnar ice detection. The noisy spectral LDR values (~~blue~~ green dots in Fig. 1c) between 0.3 ~~$m\,s^{-1}$~~ $\sim$ m s^{-1} and 1 ~~$m\,s^{-1}$~~ m s^{-1} are attributed to the low signal-to-noise ratio. Such weak impact on spectral LDR due to turbulence may be explained by the distinctively high LDR values of ice columns, which contrast to much weaker LDR signals of ice aggregates (Tyynelä et al., 2011).

4 Results

By utilizing HYDRA-W Doppler spectral observations recorded between February 2018 and April 2020, statistics of environmental conditions associated with columnar ice production were derived. All detected cloud cases within the temperature range of -10 $\sim$ 0 ~~°C~~ °C were analyzed. From the selected events the cases where significant inversion was detected, which could cause melting (e.g., Kumjian et al., 2020), were excluded. Given the data selection criteria, no rainfall or summer cloud cases were analyzed. This was done to avoid potential problems due to radar signal attenuation in rain and melting layer (Li and Moisseev, 2019). In total, 175 days of observations satisfying the data selection criteria were identified and analyzed.

4.1 Temperature and RH conditions in columnar-ice-producing regions
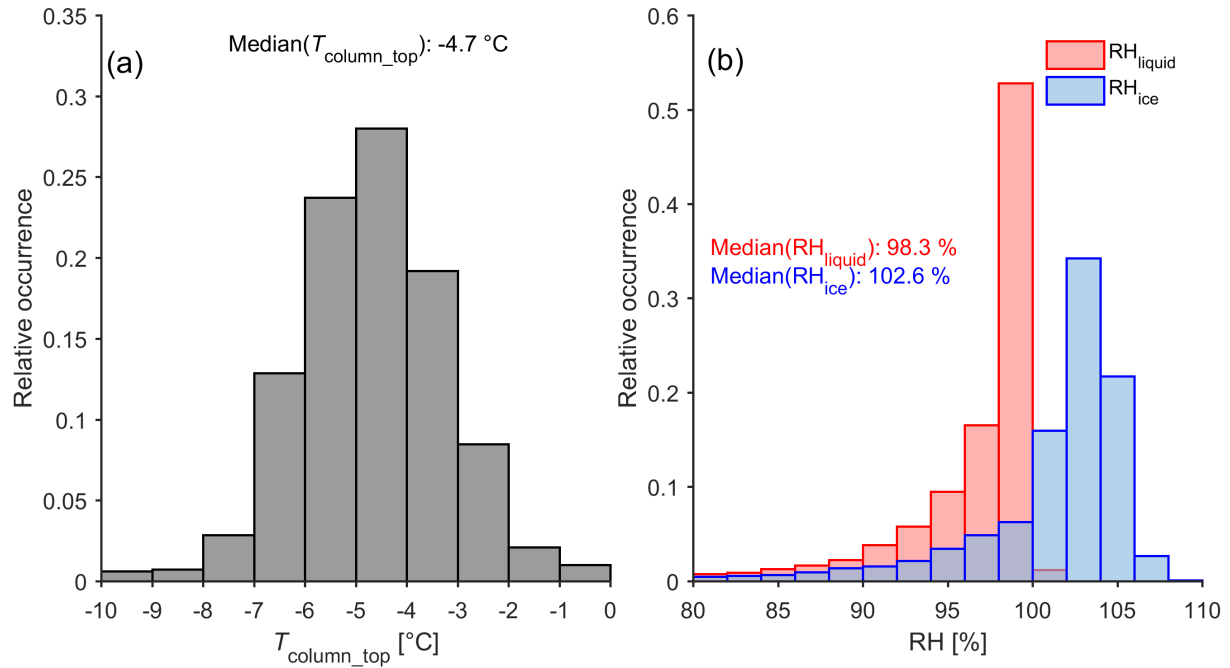
Figure 2. Statistics of (a) temperature and (b) relative humidity at H_{column_top} for all identified columnar-ice-producing cases .

Formation and growth of ice particles requires favorable environmental conditions. These conditions were assessed by using ICON forecasts, which supplemented the radar observations. Here, we define H_{column_top} as the height where ice columns are first detected, and T_{column_top} the temperature at this height. As shown in Fig. 2 (a), T_{column_top} values are mostly between -8 °C °C and -3 °C °C with the highest frequency at around -5 °C °C and a median value of -4.7 °C °C. There values are within the growth region of ice columns (Lamb and Verlinde, 2011). Such temperature distribution also bears a good resemblance to the results obtained from the early rime-splintering laboratory experiment (Hallett and Mossop, 1974) and recent statistical study (Luke et al., 2021). The statistics of humidity relative to ice (RH_{ice}) and water (RH_{liquid}) at H_{column_top} are shown in Fig. 2 (b). The median values of RH_{ice} and RH_{liquid} are 102.6 % % and 98.3 % %, respectively, indicating the supply of water vapor is sufficient for growth of ice particles. This finding is, however, not surprising, since the method detects ice columns and they are growing in this temperature regime. ~~So we can treat the~~ However, the values of RH_{liquid} and RH_{ice} should be interpreted with caution. ICON applies a liquid saturation adjustment, limiting the liquid supersaturation to saturation. RH_{liquid} values exceeding 100 % are attributed to numerical artifacts. RH_{ice} was calculated based on the forecasted temperature, pressure as well as RH_{liquid}, therefore can be affected by numerical artifacts as well. Given the uncertainty of ICON forecasts, we regard the presented statistics in Fig. 2 as a ~~"sanity"~~ "sanity" check for our method.

It should be noted that although ice columns can be detected by our method, $H_{\text{column\_top}}$ may be lower than the height where ice crystals are generated. There are two potential reasons for this. Firstly, the newly formed ice particles may be ~~spherical~~
~~(Korolev et al., 2020)~~less non-spherical (Korolev et al., 2020; Luke et al., 2021), and in this case they will have LDR values which are much smaller than our detection threshold. Secondly, at early stages of growth the radar signal of ice crystals is rather weak and does not allow accurate detection and identification of columns (Luke et al., 2021). However, the altitude difference between $H_{\text{column\_top}}$ and the actual height where columns are generated is expected to be small and not significantly affect our results.

4.2 Properties of columnar-ice-producing clouds

There are a number of questions that are associated with formation of ice crystals in clouds at these relatively warm temperatures. Above -10 ~~°C~~°C, the number concentration of INPs is expected to be small and rather uncertain (DeMott et al., 2010; Kanji et al., 2017). Therefore, it is important to know how often and in which conditions these ice crystals form. Because ice formation could be facilitated by ice particles falling from upper cloud layers, i.e. by SIP, the location where ice columns are forming, with respect to the cloud top, should be identified. Finally, the importance of the columnar ice production on surface precipitation should also be assessed.
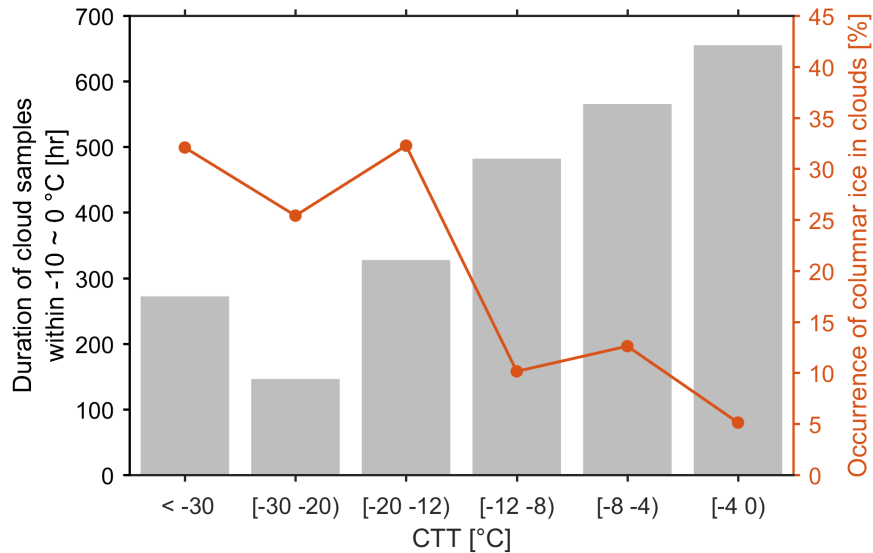
Figure 3. Duration of cloud observations (bars) and occurrence of columnar-ice-producing clouds (red dotted curve) over Hyytiälä as a function of CTT. The results were calculated based on the data collected from February 2018 to April 2020.

To identify such conditions, cloud top temperature (CTT) ~~,~~defined as the temperature of the highest detected radar return for a given measurement time ~~,~~is used. Because there are cases where several cloud layers are observed and there are gaps between these layers, typically the top of the lowest one is used. However, particles forming in the upper clouds, while not detected by

200 the radar, may seed lower cloud layers, and therefore modify their properties (Vassel et al., 2019). To limit the impact of such conditions on our analysis, following (Seifert et al., 2009) we have used radar echo gap of 2 km as the threshold which defines if the layers are connected. Recently, Proske et al. (2020) have suggested that the threshold of 2 km may overestimate the cases of cloud seeding. For this reason, we have also tried the threshold of 0.5 km to determine the cloud top, but we did not see significant changes in the results.

205   The statistics of the recorded cloud top temperatures are presented in Fig. 3. The figure (left) shows duration of detected cloud samples within the temperature of -10 $\sim$ 0 °C for a given CTT range as recorded during the observation period. Because of the focus on cold cloud cases, where the temperature in an atmospheric column does not exceed 0 °C, the observed cloud cases were recorded between October and April. The observations show that low-level clouds, i.e. clouds with warmer CTT, are relatively more frequent. This resembles the cloud occurrence statistics of (e.g., Hagihara et al., 2010; Shupe

210 et al., 2011). It appears deeper clouds, i.e. where CTT is below -12 °C, are more conducive to columnar ice production. In these cases the frequency of columnar ice occurrence is about 25 $\sim$ 33 %. For warmer clouds the frequency is lower and is around 5 $\sim$ 13 %. The average occurrence is 15 %. Interestingly, our results are comparable with a recent study by Luke et al. (2021) who have found that the occurrence of columnar ice over an Arctic site is between 10 % and 25 % depending on the temperature.
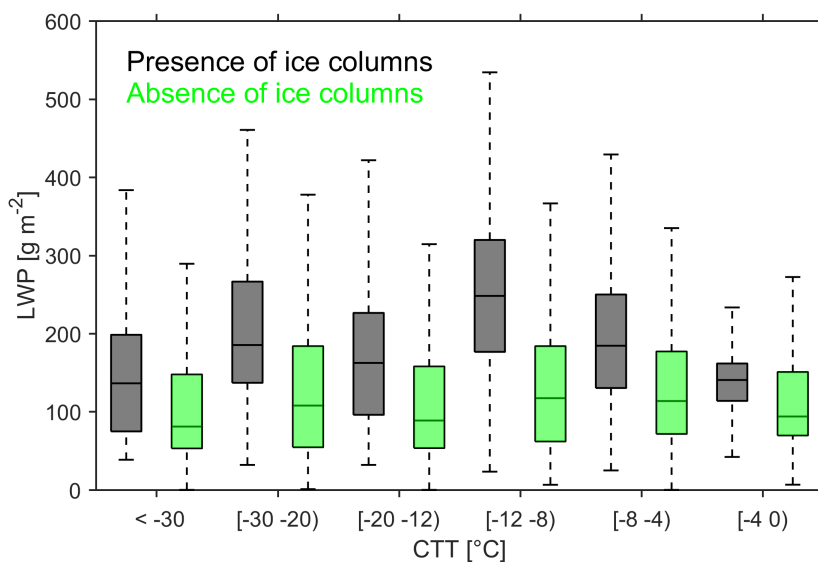
Figure 4. Comparison of LWP for clouds with and without columnar ice production. A cloud sample was identified if the cloud base was within the temperature range of -10 $\sim$ 0 °C. The boxplots represent the median (horizontal strip) and 5-95 % quantile range (whisker) of the distribution.

215   As shown in Fig. 2b, the majority of columnar ice production cases took in areas ~~of high supersaturation, which is potentially favorable for liquid water droplet formation or existence~~around liquid saturation. Although direct observations of liquid were

not available, the measurements collected by the 89 GHz passive channel in HYDRA-W allows estimation of LWP. The LWP values for the cloud cases are shown in Fig. 4. The observations show a significant amount of supercooled liquid water present in the atmospheric column. The cloud cases where ice columns were detected tend to have larger LWP values, especially where
220   CTT values were smaller than ~~-12°C~~ -8 °C. This potentially indicates that supercooled liquid droplets may play important roles in formation of ice columns. Given the mixed-phase cloud conditions, the observed columns are most probably ice needles.
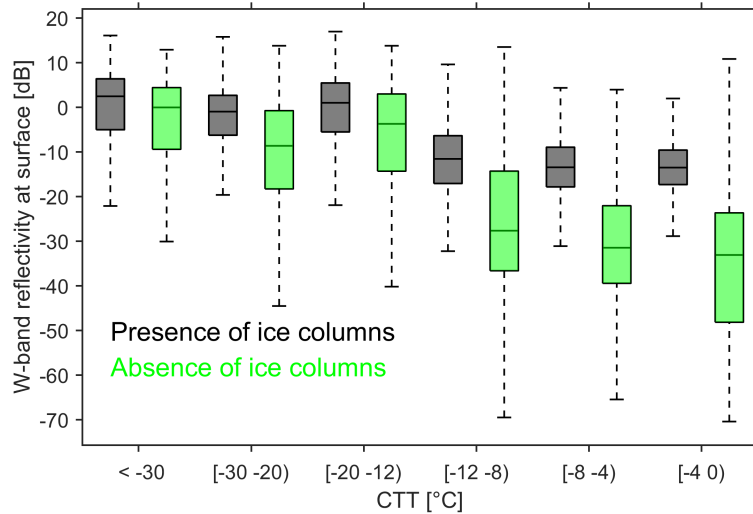
Figure 5. The same as Fig. 4 but for W-band radar reflectivity at the fourth range bin (179 m above the surface).

Formation of ice crystals is an efficient precipitation process (Lamb and Verlinde, 2011). To evaluate the impact of columnar ice production on precipitation, the radar equivalent reflectivity factor is used as the proxy for the precipitation intensity. For clouds where the radar echo extends to the ground, ~~the~~ reflectivity values at the fourth radar gate, 179 m above ground level
225   (agl), were used. As shown in Fig. 5 the reflectivity increases with decreasing CTT. This is due to the link between the cloud ~~depth~~ thickness and precipitation intensity. The columnar ice production tends to increase the precipitation intensity. This effect is more pronounced for warmer clouds, where CTT is -12 ~~°C~~ °C or warmer. In warmer clouds the precipitation intensity can be enhanced by as much as 10 fold. The factor of 10 increase in precipitation rate appears from the 10 dB increase in reflectivity (Falconi et al., 2018). As will be discussed in the next section, ~~the~~ warmer clouds tend to be single-layer clouds, where the
230   crystal formation is more directly linked to precipitation formation. ~~The colder~~ Colder clouds are prone to be consisting of the multiple cloud layers where precipitation processes are ~~more complex.~~ affected by multiple processes, such as riming, aggregation, sublimation, at various levels (e.g., Houze Jr and Medina, 2005; Verlinde et al., 2013; Moisseev et al., 2015)

4.3   Columnar ice production in single-layer and multilayered clouds

For all detected columnar-ice-producing cases, the distribution of CTT was analysed. As shown in Fig. 6 (a), ice columns can
235   form in clouds with a wide range of CTT. The majority of cases fall in the CTT range of -20 ∼ 0 ~~°C~~ °C with two peaks at

around -15 °C̶ °C and -5 °C̶ °C, respectively. The peak at around -15 °C̶ °C agrees rather well with the high occurrence of ice columns in clouds with the CTT of -20 ∼ -12 °C̶ °C (Fig. 3).
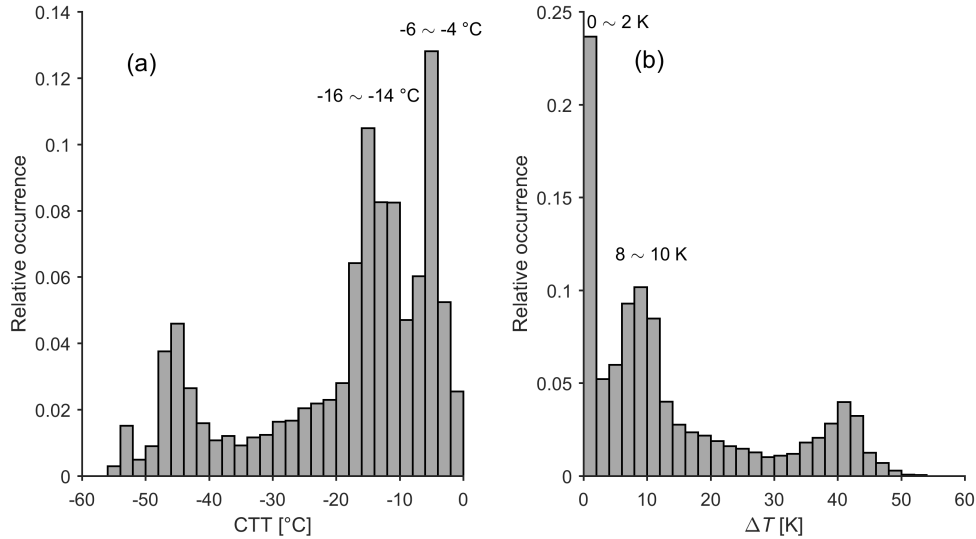
Figure 6. Relative occurrence of (a) CTT and (b) ΔT for columnar ice production cases.

Because processes responsible for the formation of ice particles in single-layer and multilayered clouds may be be different, the classification of the cloud cases was performed. Using CTT and $T_{\text{column\_top}}$, we define ΔT as the temperature difference between them. The larger ΔT is, the lower inside of the observed cloud system the columns are formed. Since The relative occurrence of ΔT also shows two peaks as presented in Fig. 6 (b). Specifically, one peak is close to $\Delta T = 0$ °C̶ K, indicating that ice columns are generated close to the cloud top. The second ΔT peak is around 10 °C̶ K.

Given the distinct distribution of ΔT, we have grouped the recorded clouds into the following three categories.

– Type 1: $\Delta T \leq 2$ °C̶ K - columnar ice production at cloud top

– Type 2: 2 °C̶ K $< \Delta T \leq 12$ °C̶ K - multilayered cloud

– Type 3: 12 °C̶ K $< \Delta T$ - multilayered cloud

Representative events of the above cloud types are presented below.

4.3.1 Columnar ice production at cloud top: $\Delta T \leq 2$ °C̶ K

This type of clouds is usually single-layer and ice columns are generated close to the cloud top. Figure 7 presents such an event on 4 November 2019. The precipitation intensity is relatively light with the CTT at around -3 °C̶ °C. The W-band reflectivity close to the surface increases to around 0 dB between 14:00 UTC and 16:00 UTC. This region coincides with the enhanced
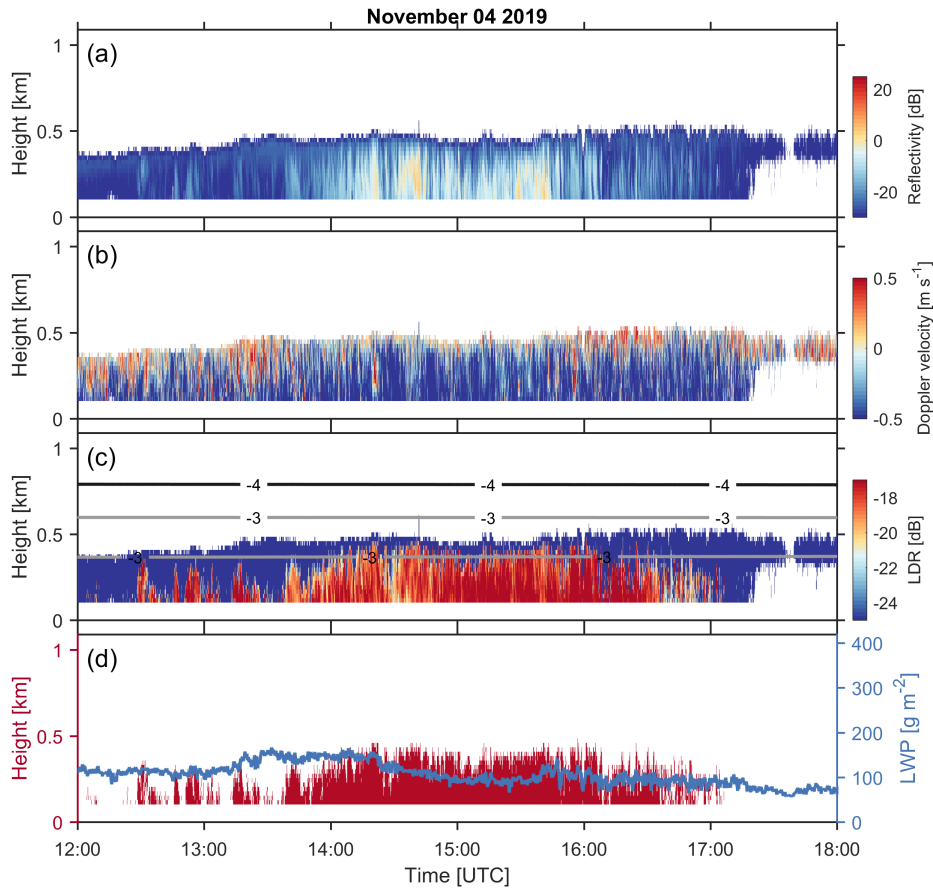
Figure 7. The columnar-ice-producing event on 4 November, 2019. HYDRA-W observations of (a) equivalent reflectivity factor, (b) mean Doppler velocity, where negative velocity indicates downward motion, and (c) LDR. Panel (d) presents the (left axis) detected columnar ice region and (right axis) LWP observed by HYDRA-W. The lines in (c) are isotherms produced by ICON.

LDR observations, which reaches values as high as -15 dB. Such high LDR values indicate that the dominant ice particle type during this period is columns. As shown in Fig. 7 (b), the cloud top is turbulent and seems to be capped by an inversion layer (Fig. 7c). The observed LWP ranges between $80 \, \mathrm{g \, m^{-2}}$ and $150 \, \mathrm{g \, m^{-2}}$. This cloud with relatively low reflectivity

255 persisted over Hyytiälä for about one day (not shown). Given the warm cloud top, the primary ice nucleation may not fully explain the significant columnar ice production (DeMott et al., 2010), as will be discussed in more detailed later. Regarding the SIP, the H-M process does not seem to be active since it requires falling ice particles serving as rimers to produce ice splinters (Hallett and Mossop, 1974).

As shown in Fig. 6, around 22 % of columnar ice production cases are attributed to single-layer shallow clouds. Bühl

260 et al. (2016) have also observed the prevalence of high LDR values for mixed-phase clouds with the CTT of -5 °C. They

speculated that these particles are formed mainly by primary ice nucleation instead of the SIP. Recently, Yang et al. (2020) have reported a similar event of shallow stratiform clouds over the tropical ocean and found that neither ~~INP~~ INPs or known SIP mechanisms can fully explain the strong production of ice particles in such clouds ~~where top temperatures were greater with top temperatures warmer~~ than -8 ~~°C~~°C. In this study, we find that ~~similar~~ such clouds also frequently occur over Hyytiälä~~.~~ , and more detailed analysis will be presented in Sec. 5.

4.3.2 Columnar ice production in multilayered clouds: 2 ~~°C~~K < ΔT ≤ 12 ~~°C~~K
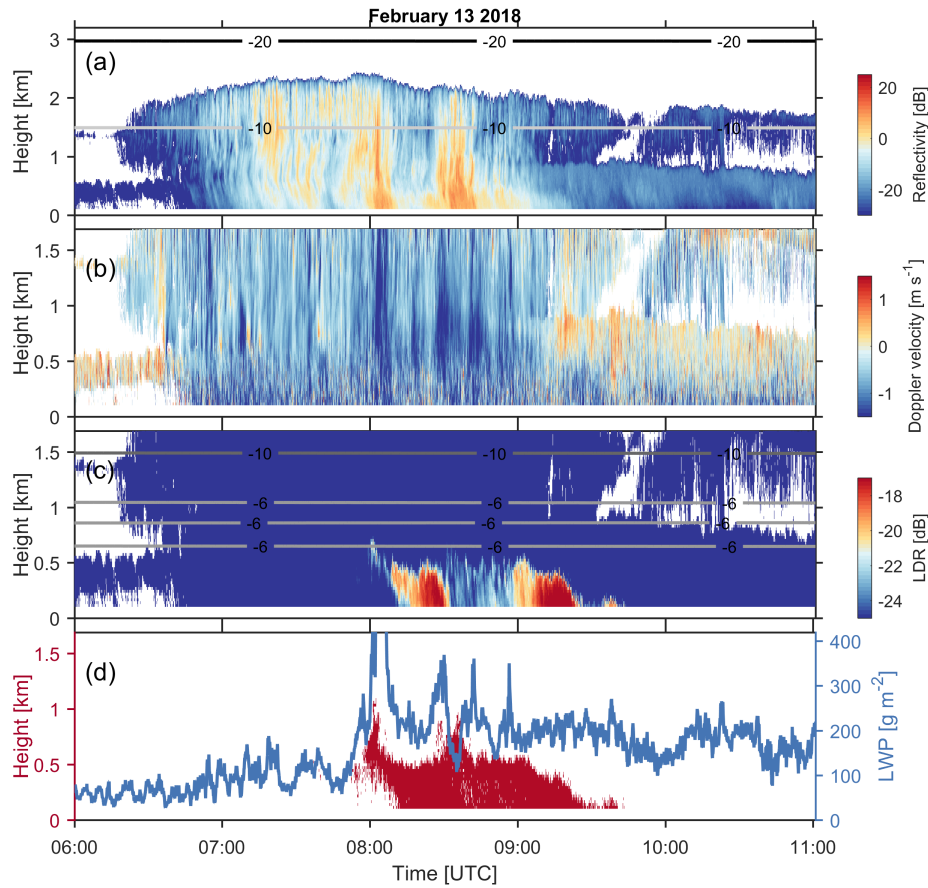
Figure 8. The columnar-ice-producing event recorded on 13 February, 2018. HYDRA-W observations of (a) equivalent reflectivity factor, (b) mean Doppler velocity, where negative velocity indicates downward motion, and (c) LDR. Panel (d) presents the (left axis) detected columnar ice region and (right axis) LWP observed by HYDRA-W. The lines in (a) and (c) are isotherms produced by ICON. Note that the y-axis scale in (a) is different from that in (b), (c) and (d).

The event that took place on 13 February 2018 is representative of the second cloud type, as defined by ΔT. As shown in Fig. 8 (a), the precipitation intensity during this event is higher than during the discussed single-layer shallow cloud case. The cloud top temperature of the upper cloud layer is about -15 $\sim$ -12 °C. Before 08:00 UTC, the observed LWP is close to 100 g m^{-2} and the mean Doppler velocity at around 0.8 km is relatively small ($\sim$ 1 m s^{-1}) which indicates that particles are unrimed or very lightly rimed. From 08:00 to 09:30 UTC, the falling snowflakes seem to be heavily rimed, as revealed by rather high LWP (from 200 g m^{-2} to over 400 g m^{-2}) and mean Doppler velocity measurements (1.2 $\sim$ 1.8 m s^{-1}) (Kneifel and Moisseev, 2020). The high LWP period coincides with the region of ice columns (Fig. 8d). During this period, the observed LDR values are enhanced, but still relatively small. This is due to masking of needle LDR signal by larger snowflakes.

This type of clouds frequently occurs over Hyytiälä (Fig. 3 and Fig. 6). Although sounding measurements were absent, this cloud type seems to very similar with the one reported by Westbrook and Illingworth (2013), namely, a layer of supercooled liquid water with the top temperature of around -15 °C seeding low-level stratus clouds in the boundary layer. In this event, the presence of supercooled liquid water may not be directly determined, however, the enhanced LWP values are indicative of the vigorously supercooled liquid water generation. In addition, the falling ice particles between 08:00 UTC and 09:30 UTC seem to be heavily rimed, as evident from mean Doppler velocity (Kneifel and Moisseev, 2020). The combination of presence of supercooled liquid water and riming indicates that the H-M process could be taking place and could be responsible for the columnar ice production.

4.3.3 Deep multilayered clouds: ΔT > 12 K

The third cloud type is not very different from the second one and represents the tail of the observed ΔT distribution as shown in Fig. 6. This type of cloud system is a deeper precipitating system with the CTT of -60 $\sim$ -40 °C, see Fig. 9 for an example . The presented case took place on 2 February 2018. There are several features that are worthwhile to point out. The mean Doppler velocity observations exhibit signatures of atmospheric waves. Between 0500 and 0600 UTC such waves can be observed at around 1 km altitude. At the later time, the wave signatures appears at 0.5 km agl. The strongest velocity variation, observed around 06:00 UTC, seem to coincide with the LWP peak. At the same time as the waves are observed signatures of columnar ice production are also detected, pointing to a possible connection between the two.

Deep precipitating clouds usually have large number of ice crystals formed at cloud top. Given the large ice flux, manifested by the higher radar reflectivity values, in this precipitation system, it is difficult for supercooled liquid droplets to survive. The supercooled water droplets can be rapidly depleted through the Wegener–Bergeron–Findeisen (WBF) process (Lamb and Verlinde, 2011; Korolev et al., 2017), as well as riming (Fukuta and Takahashi, 1999). Nevertheless, the atmospheric waves could generate conditions needed for forming and maintaining presence of supercooled liquid water droplets (Korolev, 1995; Korolev and Field, 2008; Majewski and French, 2020). Recently, Li et al. (2021) have provided radar observational evidence showing that the Kelvin-Helmholtz instability is favorable for supercooled drizzle and secondary ice production. In such cases, ice needles may be generated by the H-M process (Hogan et al., 2002; Houser and Bluestein, 2011) or freezing breakup (Luke et al., 2021; Li et al., 2021).
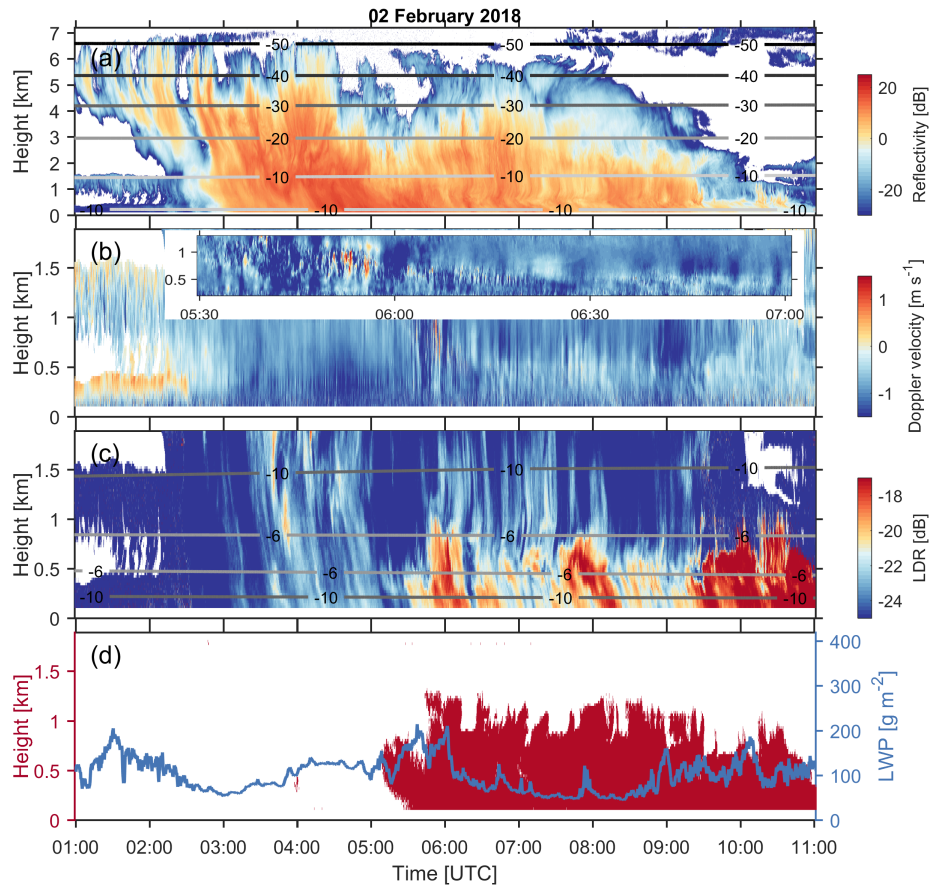
Figure 9. Same as Fig. 8, but for the columnar-ice-producing event observed on 2 February 2018. A zoom-in view on the wave signatures between 0530 and 0700 UTC is presented in (b).

4.4 Characteristics of different columnar-ice-producing cloud types

As discussed above, we have identified three types of cloud systems where columnar ice particles form. To better understand how columnar ice production is related to cloud properties, persistence of columnar ice in these clouds and the amount of LWP were considered for further analysis.

305 ### 4.4.1 Persistence of columnar ice crystals

As was demonstrated by the case studies, the columnar ice production may persist over several hours and therefore these particles may play a major role in determining cloud properties. To document this, we have derived statistics of the columnar ice production persistence for each cloud case. This was done by computing duration of a continuous columnar ice production

event. Since in some cases, for example in the presented shallow single-layer clouds (Fig. 7) formation of columns may be
310 intermittent in nature (as can also be seen in Luke et al., 2021), similar to (Shupe et al., 2011) gaps of less than 30 min were
accepted. In addition, cases persisting less than 1 min were removed. As shown in Fig. 10, 40 ∼ 50 ~~%~~ % of columnar-ice-
producing events persist for less than 1 hour. However, there is a significant fraction that could last for more than 3 or even 6
hours. This hints that the production of ice columns ~~play~~ plays an important role in defining cloud properties and should be
included while considering radiative or precipitation properties of such clouds (see for example Fig. 9).
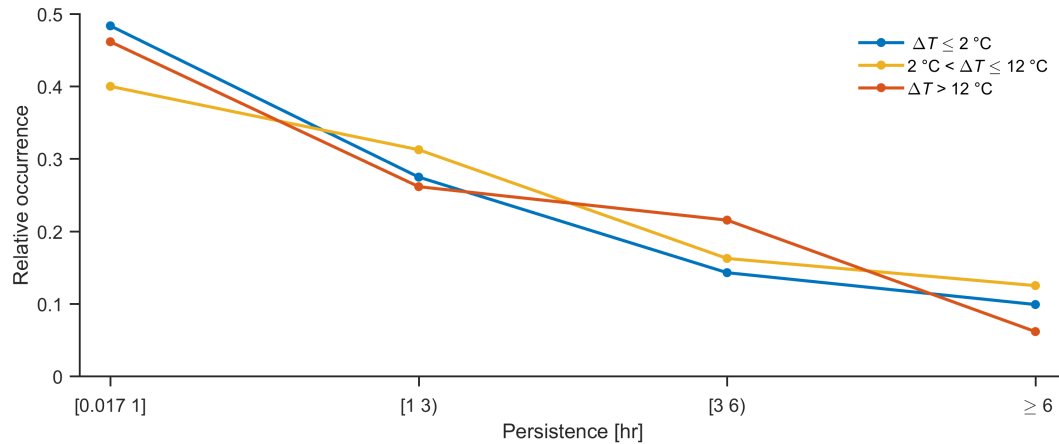
Figure 10. Relative occurrence of the persistence of columnar-ice-producing events from February 2018 to April 2020.

315 **4.4.2 LWP**

Presence of liquid water droplets may be a necessary condition for the formation of the observed ice columns. Compared to
clouds where no ice columns were detected, columnar-ice-producing clouds have higher LWP values (Fig. 4). For different
columnar-ice-producing cloud types, the observed LWP values seem to be somewhat different. Figure 11 shows LWP occur-
rence for these three cloud types. In general, their distributions are similar, while identifiable differences still exist. The median
320 value of LWP for single-layer clouds is the lowest and the second type of clouds has the highest LWP. Interestingly, while
both the second and third types of clouds are multilayered, the LWP of the second type is ~~delectably~~ detectably higher than for
the third one. Comparing Figs. 8 and 9, we find that the radar reflectivity above the columnar ice layer is generally higher in
the third cloud type than the second one. The INP concentrations in clouds with a cold top are expected to be higher than for
warmer clouds, hence more falling ice particles are expected for deep precipitating clouds. Therefore, we speculate that one of
325 the reasons responsible for the difference in LWP may be the ice number concentration, which is related to the consumption of
the liquid water via the WBF process (Lamb and Verlinde, 2011) and riming (Fukuta and Takahashi, 1999).
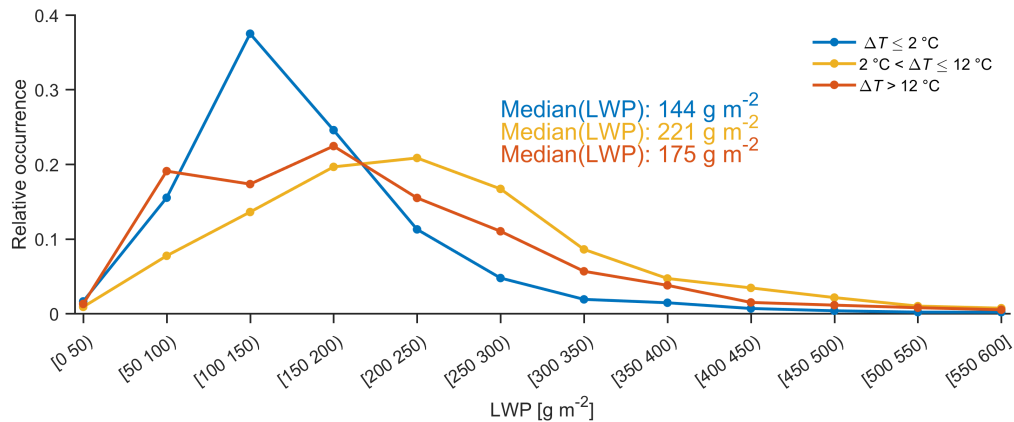
Figure 11. Relative occurrence of LWP for all columnar-ice-producing events.

5 Potential role of SIP in columnar ice production in single-layer shallow clouds

Given the rather frequent formation of ice crystals at temperatures warmer than - 10 C, where expected INP concentrations are low, it is important to investigate a potential role of SIP. In multilayered clouds, identified here as cloud types II and
330   III, ~~it has been found that~~ the ice formation can be enhanced by the H-M process (e.g., Grazioli et al., 2015; Giangrande et al., 2016; Sinclair et al., 2016; Keppas et al., 2017; Sullivan et al., 2018; Gehring et al., 2020), among other mechanisms (Korolev and Leisner, 2020). In single-layer clouds the mechanisms for ice multiplication are less ~~investigated. Recent studies by Lauber et al. (2018); Keinert et al. (2020); Lauber et al. (2021)~~ established. However, recent studies by Lauber et al. (2018); Keinert et a have shown that freezing fragmentation may play such a role. To study if these columnar ice particles can be attributed to
335   the SIP, the estimated ice number concentrations are compared to the expected INP concentrations. If the derived ~~number concentrations of ice exceed those~~ ice number concentrations exceed these of INPs, we can conclude that the SIP is potentially active in such clouds. The concentration of INP was computed by using CTT ~~using different parameterizations reported in literature~~in different paramterizations, i.e.

- Fletcher (1962) parameterization based on INP measurements obtained below -10 ~~°C~~°C.

340   - Cooper (1986) parameterization which is not directly derived from INP measurements but the observed ice number concentrations when the impact of SIP is minimized. The temperature of measurements is between -30 ~~°C~~°C and -5 ~~°C~~°C.

- DeMott et al. (2010) parameterization based on INP measurements from 9 sites between -35 ~~°C~~°C and -9 ~~°C~~°C. In our study we have used the average INP concentration - temperature relation presented in DeMott et al. (2010).

345   - Schneider et al. (2020) parameterization derived from the INP measurements obtained at Hyytiälä. The temperature range is -20 $\sim$ -8 ~~°C~~°C. Also from this study the average INP concentration - temperature relation was used.

As was previously discussed, the INP parameterizations differ significantly at this temperatures (-10 ∼ 0 °C), as shown in Fig. 12. It should be noted that not all parameterizations were derived using observations at these cloud temperatures and some of them were extrapolated beyond their validity range. The most interesting comparison is to (Schneider et al., 2020), which is based on observations at Hyytiälä collected during 2018, so their observation period at least partially overlaps with ours. It should also be pointed out that INP observations were carried out at the ground, where INP concentrations are typically higher.

~~Probability density function (PDF) of estimated columnar ice (left) and INP (right) concentrations in shallow single-layer clouds.~~

Radar-based retrieval of particle number concentration is rather uncertain. Because of this uncertainty, the derived number concentrations should be treated as our best estimates of the order of magnitude of the ice column number concentration. As shown in Fig. 4, the observed LWP for columnar-ice-producing clouds is significantly higher than those without ice columns. Hence, pristine ice crystals are anticipated to grow in mixed-phase conditions and ice needles rather than solid columns are expected to form (Lamb and Verlinde, 2011). This limits the parameter space, where we need to search for microphysical properties of ice particles to constrain our retrieval.

The retrieval is based on estimating ice water content from radar observations, following (Hogan et al., 2006), as:

$$\text{IWC} = 0.00058ZT + 0.0923Z - 0.00706T - 0.992 \; \underline{g \; m^{-3}} [\text{g m}^{-2}], \tag{1}$$

where Z is the W-band radar reflectivity and T is the air temperature. Because, in a single-layer shallow cloud ($\Delta T \leq 2$ ~~°C~~°C), ice needles are the predominant precipitation particles, radar reflectivity measured close to the ground, in the fourth radar gate, 329 m amsl or 179 m agl, is used in this retrieval. The selection of the reflectivity measured close to the ground helps to limit potential attenuation problems, as well. Using IWC the number concentration of ice needles, N_{needle}, can be estimated as follows (Li et al., 2021):

$$N_{\text{needle}} = \frac{\text{IWC}}{m_{\text{needle}}} \tag{2}$$

where m_{needle} is mass of a characteristic ice needle. The introduced uncertainty at this step depends on the definition of the characteristic needle. Here, we use mean Doppler velocity (MDV) and velocity-mass relation to estimate m_{needle}. Since MDV is reflectivity weighted, m_{needle} would be mainly determined by larger ice particles, and therefore the resulting N_{needle} is underestimated. For the purpose of this study, this underestimation is not a major issue, because we want to test if the observed N_{needle} exceeds expected INP concentrations.

There are a number of reported ice needle properties. To take into account potential differences in ice needle properties, two relations linking velocity and mass by Kajikawa (1976) for rimed needles, and (Heymsfield, 1972) for unrimed needles were used. For rimed ice needles, the relation between terminal fall velocity and mass was derived by Kajikawa (1976) and can be written as:

$$v_{\text{needle, rimed}} = 1.55 m_{\text{needle, rimed}}^{0.271} \left[\frac{\rho(z)}{\rho(1024 \text{ m})} \right]^{0.4} \underline{m \; s^{-1}} [\text{m s}^{-1}] \tag{3}$$

where $m_{\text{needle, rimed}}$ is the mass of rimed ice needles, and the term $\left[\frac{\rho(z)}{\rho(1024\,\text{m})}\right]^{0.4}$ accounts for the change in air density ρ at a given height z (Heymsfield et al., 2007). In our study z is 329 m and in Kajikawa (1976) the altitude where needles were observed is 1024 m. For unrimed needles, Heymsfield (1972) has derived a relation linking terminal fall velocity and needle length, L. The terminal velocity of unrimed needles at a given height can be estimated as follows (Heymsfield, 1972):

$$v_{\text{needle, unrimed}} = \left(0.0006 + 0.2796L - 0.0497L^2 + 0.0041L^3\right)\left[\frac{\rho(z)}{\rho(0\,\text{m})}\right]^{0.4} ~~m~s^{-1}~[\text{m s}^{-1}] \tag{4}$$

The needle can be modeled as a cylinder, the mass of which is:

$$m_{\text{needle, unrimed}} = \frac{\pi}{4}\rho_{\text{ice}} L D^2 \tag{5}$$

where ρ_{ice} [~~g cm^{-3}~~ g cm^{-3}] and D [~~mm~~ mm] denote density of unrimed needles and the minor axis, respectively. Their parameterizations have been given by Heymsfield (1972):

$$\rho_{\text{ice}} = 0.6L^{-0.117} \tag{6}$$

and

$$D = 0.1973L^{0.414}. \tag{7}$$

Applying the power law fit to $m_{\text{needle, unrimed}}$ and $v_{\text{needle, unrimed}}$ values when $L \in$ ~~[0.03 5]~~ [0.03, 5] [~~mm~~ mm] yields:

$$v_{\text{needle, unrimed}} = 1.09 m_{\text{needle, unrimed}}^{0.377}\left[\frac{\rho(z)}{\rho(0\,\text{m})}\right]^{0.4}. \tag{8}$$

The observed MDV is affected by vertical air motion. To at least partially mitigate this issue, the observed MDV is averaged over 20 min (Protat and Williams, 2011; Mosimann, 1995; Kneifel and Moisseev, 2020; Silber et al., 2020). While this step reduces impact of air motion by averaging Doppler velocity over updrafts and downdrafts, the residual air motion is expected to widen the retrieved distribution of N_{needle}.

The derived number concentrations of ice particles are compared to expected INP concentrations (Fig. 12). The results show that the estimated ice number concentrations for ~~the~~ rimed needles (Kajikawa, 1976) is generally larger than that of unrimed (Heymsfield, 1972). Regardless of the difference between rimed and unrimed needles, and INP parameterization used, there seems to be a large fraction of ~~the~~ cases where INP concentrations are not sufficient to explain observed N_{needle}. Our results are similar to the conclusion reached by (Luke et al., 2021), who have used a different approach for the establishing the range of ice crystal concentration from radar observations. ~~For many cases~~ As shown in Fig. 12, the majority of N_{needle} ~~is in the order of $10^{-2} \sim 10^1$ L^{-1}~~ values fall in the range of $10^{-2} \sim 10^1$ L^{-1}, which is similar with ~~the number observed~~ aircraft measurements obtained in tropical stratiform clouds (Yang et al., 2020).

The significant discrepancy between INP concentrations estimated from INP parameterizations and retrieved ice number concentrations indicates that primary ice nucleation does not seem to be the only mechanism responsible for the formation of
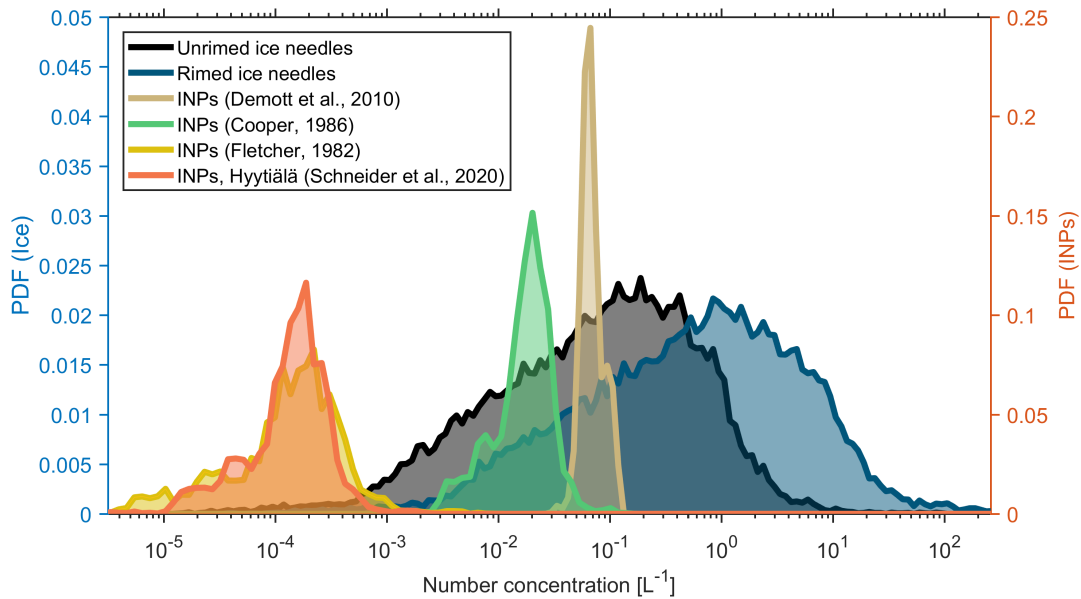
Figure 12. Probability density function (PDF) of estimated columnar ice (left) and INP (right) concentrations in shallow single-layer clouds.

ice particles in these shallow clouds. Because, the analysis was performed on shallow single-layer clouds, this discrepancy may not be explained by the H-M process (Hallett and Mossop, 1974) since no rimers are falling from upper clouds. So it appears that other, less studied, SIP mechanisms may play an important role in amplifying ice number concentrations in such shallow clouds. This conclusion is inline with a number of other studies. For example, Knight (2012) ~~have~~ has found that the SIP may take place at -5 ~~°~~°C at the absence of rimers, for which the cause is still under investigation. Recently, similar finding reported for stratiform clouds over the tropical ocean by Yang et al. (2020). They have speculated that droplet collisional freezing (Hobbs, 1965; Alkezweeny, 1969) and pre-activated INPs (Roberts and Hallett, 1968; Mossop, 1970) could be responsible for this discrepancy. Recent laboratory studies (Lauber et al., 2018; Keinert et al., 2020) have shown that freezing breakup may be a source of secondary ice particles. Luke et al. (2021) have also suggested that freezing breakup may be more efficient than the H-M process in nature.

6 Conclusions

This study documents formation of ice particles in clouds at the temperatures of -10 ~~°C or higher~~°C or warmer. The analysis was performed using W-band cloud radar observations collected at the University of Helsinki Hyytiälä station starting from February 2018 ~~to~~ through April 2020. The columnar ice particles were identified using measurements of spectral LDR. It was found that ~~ice particle~~ columnar ice formation is relatively frequent in ~~such clouds . The radar observations detect formation of~~ ~~ice particles in~~ clouds at temperatures of -10 °C or warmer. The occurrence frequency of columnar ice particles is 5 ∼ 13 ~~% of~~

~~clouds , where cloud top temperature is~~ % in clouds with top temperatures exceeding -12 ~~°C or warmer~~°C. In colder clouds, this percentage can be as high as 33 ~~%~~%. The columnar ice producing clouds tend to have higher LWP, potentially indicating that supercooled water droplets are important for formation of the observed ice particles. It was also observed that columnar ice production ~~seems~~ seem to have a significant impact on the surface precipitation. This effect is especially important for warmer clouds.

Using the temperature difference, ΔT, between the altitudes where columns are first detected and cloud top, the columnar-ice-producing clouds were subdivided into three categories. First category, where ΔT is less or equal to 2 ~~°C~~K , represents shallow single-layer clouds. In these clouds ice particles are forming at or close to the cloud top. The other two categories, where 2 ~~°C~~K $< \Delta T \leq$ 12 ~~°C~~K and $\Delta T >$ 12 ~~°C~~K , represent deeper multi-layered clouds. In multi-layered cloud systems, columnar ice crystals are forming in lower cloud layer seeded by ice particles falling from upper cloud levels. It was observed that $40 \sim 50$ ~~%~~% of columnar ice production cases persist for 1 hour or less, while in some cases they can persist for over 6 hours. The distributions of LWP values for the three types of columnar-ice-producing clouds are somewhat different. The median LWP value is the largest (221 ~~$g\,m^{-2}$~~$\mathrm{g\,m^{-2}}$) in clouds where 2 ~~°C~~K $< \Delta T \leq$ 12 ~~°C~~K. Such high LWP could favor riming and cause Hallet-Mossop process. To make a definite conclusion, however, a more thorough study, where locations of supercooled liquid layers is identified, is needed. For the single-layer shallow clouds, number concentrations of ice columns were derived from the radar observations. It was observed that the concentration of ice particles exceeds expected concentration of INP for a large number of cases. This indicates that a SIP mechanism is active in these clouds. Given that in single-layer shallow clouds, there are no rimers that could cause H-M process, we advocate that another SIP process may play a role here.

Data availability. W-band radar data are available from https://doi.org/10.23729/5aab6b78-90c9-49ab-8264-f4168528a0f3. ICON data are generated by the European Research Infrastructure for the observation of Aerosol, Clouds and Trace Gases (ACTRIS) and are available from the ACTRIS Data Centre using the following link: https://hdl.handle.net/21.12132/2.fdcadfd7b8ac4c4d.

Author contributions. DM conceptualized the study. HL performed the investigation and wrote the draft. OM, PT and DM contributed to reviewing and editing this draft.

Competing interests. The authors declare that they have no conflict of interest.

Acknowledgements. We would like to thank the personnel of Hyytiälä station for their support in field observation. ~~We want to acknowledge Matti Leskinen~~ Matti Leskinen is acknowledged for his work in radar maintenance. We want to thank Dr Anniina Korpinen, Dr Simo Tukiainen and Dr Axel Seifert for helpful discussions on ICON forecasts. This research has been supported by the Horizon 2020 (grant nos. ~~ACTRIS-2 654109~~ACTRIS-2654109, ACTRIS PPP 739530, ACTRIS-IMP 871115, ATMO-ACCESS 101008004, ERA-PLANET iCUPE,

450 689443) and Academy of Finland (ACTRIS-NF 328616, ACTRIS-CF 329274, NanoBioMass 307537, ACRoBEAR 334792, and Center of Excellence in Atmospheric Sciences, 307331, Atmosphere and Climate Competence Center, 337549), University of Helsinki (ACTRIS-HY). ~~Haoran Li was also funded by China Scholarship Council.~~

We acknowledge the European Research Infrastructure for the observation of Aerosol, Clouds and Trace Gases (ACTRIS) for providing the DWD ICON (Global) model data, which was produced by the ~~Deutscher Wetterdienst (DWD)~~ DWD and the Finnish Meteorological

455 Institute, and is available for download from https://cloudnet.fmi.fi/. ACTRIS has received funding from the European Union's Horizon 2020 research and innovation programme under grant agreement No 654109.

References

Alkezweeny, A.: Freezing of supercooled water droplets due to collision, Journal of Applied Meteorology, 8, 994–995, 1969.

Aydin, K. and Walsh, T. M.: Millimeter wave scattering from spatial and planar bullet rosettes, IEEE transactions on geoscience and remote sensing, 37, 1138–1150, 1999.

Barthazy, E. and Schefold, R.: Fall velocity of snowflakes of different riming degree and crystal types, Atmospheric research, 82, 391–398, 2006.

Beard, K. V.: Ice initiation in warm-base convective clouds: An assessment of microphysical mechanisms, Atmospheric research, 28, 125–152, 1992.

Bringi, V. N. and Chandrasekar, V.: Polarimetric Doppler weather radar: principles and applications, Cambridge university press, 2001.

Bühl, J., Seifert, P., Myagkov, A., and Ansmann, A.: Measuring ice-and liquid-water properties in mixed-phase cloud layers at the Leipzig Cloudnet station, Atmos. Chem. Phys, 16, 10 609–10 620, 2016.

CLU: Icon-iglo-12-23, icon-iglo-36-47, gdas1 model data; 2018-02-01 to 2020-04-30; from Hyytiälä. Generated by the cloud profiling unit of the ACTRIS Data Centre,, https://hdl.handle.net/21.12132/2.fdcadfd7b8ac4c4d., 2021.

Cooper, W. A.: Ice initiation in natural clouds, Springer, 1986.

DeMott, P. J., Prenni, A. J., Liu, X., Kreidenweis, S. M., Petters, M. D., Twohy, C. H., Richardson, M., Eidhammer, T., and Rogers, D.: Predicting global atmospheric ice nuclei distributions and their impacts on climate, Proceedings of the National Academy of Sciences, 107, 11 217–11 222, 2010.

DeMott, P. J., Hill, T. C., McCluskey, C. S., Prather, K. A., Collins, D. B., Sullivan, R. C., Ruppel, M. J., Mason, R. H., Irish, V. E., Lee, T., et al.: Sea spray aerosol as a unique source of ice nucleating particles, Proceedings of the National Academy of Sciences, 113, 5797–5803, 2016.

Dye, J. and Hobbs, P.: Effect of carbon dioxide on the shattering of freezing water drops, Nature, 209, 464–466, 1966.

Evans, D. and Hutchinson, W.: The electrification of freezing water droplets and of colliding ice particles, Quarterly Journal of the Royal Meteorological Society, 89, 370–375, 1963.

Falconi, M. T., Lerber, A. v., Ori, D., Marzano, F. S., and Moisseev, D.: Snowfall retrieval at X, Ka and W bands: consistency of backscattering and microphysical properties using BAECC ground-based measurements, Atmospheric Measurement Techniques, 11, 3059–3079, 2018.

Field, P. R., Lawson, R. P., Brown, P. R., Lloyd, G., Westbrook, C., Moisseev, D., Miltenberger, A., Nenes, A., Blyth, A., Choularton, T., et al.: Secondary ice production: Current state of the science and recommendations for the future, Meteorological Monographs, 58, 7–1, 2017.

Findeisen, W. and Findeisen, E.: Untersuchungen uber die Eissplitterbildung an Reifschichten (Ein Beitrag zur Frage der Entstehung der Gewitterelektrizitat und zur Mikrostruktur der Cumulonimben), Meteor. Z, 60, 145–154, 1943.

Fletcher, N. H.: The physics of rainclouds, Cambridge University Press, 1962.

Fridlind, A. M., Ackerman, A., McFarquhar, G., Zhang, G., Poellot, M., DeMott, P., Prenni, A., and Heymsfield, A.: Ice properties of single-layer stratocumulus during the Mixed-Phase Arctic Cloud Experiment: 2. Model results, Journal of Geophysical Research: Atmospheres, 112, 2007.

Fukuta, N. and Takahashi, T.: The Growth of Atmospheric Ice Crystals: A Summary of Findings in Vertical Supercooled Cloud Tunnel Studies, Journal of the Atmospheric Sciences, 56, 1963 – 1979, https://doi.org/10.1175/1520-0469(1999)056<1963:TGOAIC>2.0.CO;2, 1999.

Gehring, J., Oertel, A., Vignon, E., Jullien, N., Besic, N., and Berne, A.: Microphysics and dynamics of snowfall associated with a warm
conveyor belt over Korea, Atmospheric Chemistry and Physics, 20, 7373–7392, https://doi.org/10.5194/acp-20-7373-2020, 2020.

Giangrande, S. E., Toto, T., Bansemer, A., Kumjian, M. R., Mishra, S., and Ryzhkov, A. V.: Insights into riming and aggregation processes
as revealed by aircraft, radar, and disdrometer observations for a 27 April 2011 widespread precipitation event, Journal of Geophysical
Research: Atmospheres, 121, 5846–5863, 2016.

Grazioli, J., Lloyd, G., Panziera, L., Hoyle, C. R., Connolly, P. J., Henneberger, J., and Berne, A.: Polarimetric radar and in situ
observations of riming and snowfall microphysics during CLACE 2014, Atmospheric Chemistry and Physics, 15, 13 787–13 802,
https://doi.org/10.5194/acp-15-13787-2015, 2015.

Hagihara, Y., Okamoto, H., and Yoshida, R.: Development of a combined CloudSat-CALIPSO cloud mask to show global cloud distribution,
Journal of Geophysical Research: Atmospheres, 115, 2010.

Hallett, J. and Mossop, S.: Production of secondary ice particles during the riming process, Nature, 249, 26–28, 1974.

Hari, P. and Kulmala, M.: Station for measuring ecosystem-atmosphere relations: (SMEAR II), in: Boreal Environment Research,, vol. 10,
pp. 315–322, Springer, 2005.

Heymsfield, A.: Ice crystal terminal velocities, Journal of the Atmospheric Sciences, 29, 1348–1357, 1972.

Heymsfield, A. J., Bansemer, A., and Twohy, C. H.: Refinements to ice particle mass dimensional and terminal velocity relationships for ice
clouds. Part I: Temperature dependence, Journal of the Atmospheric Sciences, 64, 1047–1067, 2007.

Hoarau, T., Pinty, J.-P., and Barthe, C.: A representation of the collisional ice break-up process in the two-moment microphysics LIMA v1.
0 scheme of Meso-NH, Geoscientific Model Development, 11, 4269–4289, 2018.

Hobbs, P.: The aggregation of ice particles in clouds and fogs at low temperatures, Journal of the Atmospheric Sciences, 22, 296–300, 1965.

Hobbs, P. V. and Rangno, A. L.: Ice particle concentrations in clouds, Journal of the atmospheric sciences, 42, 2523–2549, 1985.

Hobbs, P. V. and Rangno, A. L.: Rapid development of high ice particle concentrations in small polar maritime cumuliform clouds, Journal
of the atmospheric sciences, 47, 2710–2722, 1990.

Hogan, R., Field, P., Illingworth, A., Cotton, R., and Choularton, T.: Properties of embedded convection in warm-frontal mixed-phase cloud
from aircraft and polarimetric radar, Quarterly Journal of the Royal Meteorological Society, 128, 451–476, 2002.

Hogan, R. J., Mittermaier, M. P., and Illingworth, A. J.: The retrieval of ice water content from radar reflectivity factor and temperature and
its use in evaluating a mesoscale model, Journal of Applied Meteorology and Climatology, 45, 301–317, 2006.

Houser, J. L. and Bluestein, H. B.: Polarimetric Doppler radar observations of Kelvin–Helmholtz waves in a winter storm, Journal of the
atmospheric sciences, 68, 1676–1702, 2011.

Houze Jr, R. A. and Medina, S.: Turbulence as a mechanism for orographic precipitation enhancement, Journal of the atmospheric sciences,
62, 3599–3623, 2005.

Kajikawa, M.: Observation of falling motion of columnar snow crystals, Journal of the Meteorological Society of Japan. Ser. II, 54, 276–284,
1976.

Kalesse, H. and Luke, E.: Development and validation of a supervised machine learning radar Doppler spectra peak-finding algorithm,
Atmospheric Measurement Techniques, 12, 2019.

Kalesse, H., Szyrmer, W., Kneifel, S., Kollias, P., and Luke, E.: Fingerprints of a riming event on cloud radar Doppler spectra: observations
and modeling, Atmos. Chem. Phys, 16, 2997–3012, 2016.

Kanji, Z. A., Ladino, L. A., Wex, H., Boose, Y., Burkert-Kohn, M., Cziczo, D. J., and Krämer, M.: Overview of ice nucleating particles,
Meteorological Monographs, 58, 1–1, 2017.

Keinert, A., Spannagel, D., Leisner, T., and Kiselev, A.: Secondary Ice Production upon Freezing of Freely Falling Drizzle Droplets, Journal of the Atmospheric Sciences, 77, 2959 – 2967, https://doi.org/10.1175/JAS-D-20-0081.1, 2020.

Keppas, S. C., Crosier, J., Choularton, T., and Bower, K.: Ice lollies: An ice particle generated in supercooled conveyor belts, Geophysical Research Letters, 44, 5222–5230, 2017.

Kneifel, S. and Moisseev, D.: Long-Term Statistics of Riming in Nonconvective Clouds Derived from Ground-Based Doppler Cloud Radar Observations, Journal of the Atmospheric Sciences, 77, 3495–3508, 2020.

Knight, C. A.: Ice growth from the vapor at- 5° C, Journal of the atmospheric sciences, 69, 2031–2040, 2012.

Koenig, L. R.: The glaciating behavior of small cumulonimbus clouds, Journal of the Atmospheric Sciences, 20, 29–47, 1963.

Kollias, P., Rémillard, J., Luke, E., and Szyrmer, W.: Cloud radar Doppler spectra in drizzling stratiform clouds: 1. Forward modeling and remote sensing applications, Journal of Geophysical Research: Atmospheres, 116, 2011.

Korolev, A. and Field, P. R.: The effect of dynamics on mixed-phase clouds: Theoretical considerations, Journal of the Atmospheric Sciences, 65, 66–86, 2008.

Korolev, A. and Leisner, T.: Review of experimental studies of secondary ice production, Atmospheric Chemistry and Physics, 20, 11 767–11 797, 2020.

Korolev, A., McFarquhar, G., Field, P. R., Franklin, C., Lawson, P., Wang, Z., Williams, E., Abel, S. J., Axisa, D., Borrmann, S., et al.: Mixed-phase clouds: Progress and challenges, Meteorological Monographs, 58, 5–1, 2017.

Korolev, A., Heckman, I., Wolde, M., Ackerman, A. S., Fridlind, A. M., Ladino, L. A., Lawson, R. P., Milbrandt, J., and Williams, E.: A new look at the environmental conditions favorable to secondary ice production, Atmospheric Chemistry and Physics, 20, 1391–1429, https://doi.org/10.5194/acp-20-1391-2020, 2020.

Korolev, A. V.: The influence of supersaturation fluctuations on droplet size spectra formation, Journal of the atmospheric sciences, 52, 3620–3634, 1995.

Küchler, N., Kneifel, S., Löhnert, U., Kollias, P., Czekala, H., and Rose, T.: A W-band radar–radiometer system for accurate and continuous monitoring of clouds and precipitation, Journal of Atmospheric and Oceanic Technology, 34, 2375–2392, 2017.

Kumjian, M. R., Tobin, D. M., Oue, M., and Kollias, P.: Microphysical Insights into Ice Pellet Formation Revealed by Fully Polarimetric Ka-Band Doppler Radar, Journal of Applied Meteorology and Climatology, 59, 1557–1580, 2020.

Lamb, D. and Verlinde, J.: Physics and chemistry of clouds, Cambridge University Press, 2011.

Lauber, A., Kiselev, A., Pander, T., Handmann, P., and Leisner, T.: Secondary ice formation during freezing of levitated droplets, Journal of the Atmospheric Sciences, 75, 2815–2826, 2018.

Lauber, A., Henneberger, J., Mignani, C., Ramelli, F., Pasquier, J. T., Wieder, J., Hervo, M., and Lohmann, U.: Continuous secondary-ice production initiated by updrafts through the melting layer in mountainous regions, Atmospheric Chemistry and Physics, 21, 3855–3870, https://doi.org/10.5194/acp-21-3855-2021, 2021.

Li, H. and Moisseev, D.: Melting layer attenuation at Ka- and W-bands as derived from multi-frequency radar Doppler spectra observations, Journal of Geophysical Research: Atmospheres, 124, https://doi.org/10.1029/2019JD030316, 2019.

Li, H. and Moisseev, D.: Two layers of melting ice particles within a single radar bright band: Interpretation and implications, Geophysical Research Letters, 47, e2020GL087 499, 2020.

Li, H., Moisseev, D., and von Lerber, A.: How does riming affect dual-polarization radar observations and snowflake shape?, Journal of Geophysical Research: Atmospheres, 123, 6070–6081, 2018.

Li, H., Tiira, J., von Lerber, A., and Moisseev, D.: Towards the connection between snow microphysics and melting layer: insights from multifrequency and dual-polarization radar observations during BAECC, Atmospheric Chemistry and Physics, 20, 9547–9562, 2020.

Li, H., Korolev, A., and Moisseev, D.: Supercooled liquid water and secondary ice production in Kelvin-Helmholtz instability as revealed by radar Doppler spectra observations, Atmospheric Chemistry and Physics Discussions, 2021, 1–22, https://doi.org/10.5194/acp-2021-338, 2021.

Locatelli, J. D. and Hobbs, P. V.: Fall speeds and masses of solid precipitation particles, Journal of Geophysical Research, 79, 2185–2197, 1974.

Luke, E. P., Kollias, P., and Shupe, M. D.: Detection of supercooled liquid in mixed-phase clouds using radar Doppler spectra, Journal of Geophysical Research: Atmospheres, 115, 2010.

Luke, E. P., Yang, F., Kollias, P., Vogelmann, A. M., and Maahn, M.: New insights into ice multiplication using remote-sensing observations of slightly supercooled mixed-phase clouds in the Arctic, Proceedings of the National Academy of Sciences, 118, https://doi.org/10.1073/pnas.2021387118, 2021.

Majewski, A. and French, J. R.: Supercooled drizzle development in response to semi-coherent vertical velocity fluctuations within an orographic-layer cloud., Atmospheric Chemistry & Physics, 20, 2020.

Matrosov, S. Y., Reinking, R. F., Kropfli, R. A., Martner, B. E., and Bartram, B.: On the use of radar depolarization ratios for estimating shapes of ice hydrometeors in winter clouds, Journal of Applied Meteorology, 40, 479–490, 2001.

McCluskey, C. S., Ovadnevaite, J., Rinaldi, M., Atkinson, J., Belosi, F., Ceburnis, D., Marullo, S., Hill, T. C., Lohmann, U., Kanji, Z. A., et al.: Marine and terrestrial organic ice-nucleating particles in pristine marine to continentally influenced Northeast Atlantic air masses, Journal of Geophysical Research: Atmospheres, 123, 6196–6212, 2018.

Moisseev, D. N.: Hyytiala W-band cloud radar 2017-2019 [Data set], https://etsin.fairdata.fi/dataset/1583dc19-1cb8-441f-b336-22858b366cb1, 2020.

Moisseev, D. N., Unal, C. M., Russchenberg, H. W., and Ligthart, L. P.: Improved polarimetric calibration for atmospheric radars, Journal of Atmospheric and Oceanic Technology, 19, 1968–1977, 2002.

Moisseev, D. N., Lautaportti, S., Tyynela, J., and Lim, S.: Dual-polarization radar signatures in snowstorms: Role of snowflake aggregation, Journal of Geophysical Research: Atmospheres, 120, 12 644–12 655, 2015.

Morrison, H., Curry, J., and Khvorostyanov, V.: A new double-moment microphysics parameterization for application in cloud and climate models. Part I: Description, Journal of the atmospheric sciences, 62, 1665–1677, 2005.

Mosimann, L.: An improved method for determining the degree of snow crystal riming by vertical Doppler radar, Atmospheric research, 37, 305–323, 1995.

Mossop, S.: Concentrations of ice crystals in clouds, Bulletin of the American Meteorological Society, 51, 474–480, 1970.

Mossop, S.: The origin and concentration of ice crystals in clouds, Bulletin of the American Meteorological Society, 66, 264–273, 1985.

Myagkov, A., Seifert, P., Bauer-Pfundstein, M., and Wandinger, U.: Cloud radar with hybrid mode towards estimation of shape and orientation of ice crystals, Atmospheric Measurement Techniques, 9, 469–489, 2016a.

Myagkov, A., Seifert, P., Wandinger, U., Bühl, J., and Engelmann, R.: Relationship between temperature and apparent shape of pristine ice crystals derived from polarimetric cloud radar observations during the ACCEPT campaign, Atmospheric Measurement Techniques, 9, 3739–3754, 2016b.

605 Niemand, M., Möhler, O., Vogel, B., Vogel, H., Hoose, C., Connolly, P., Klein, H., Bingemer, H., DeMott, P., Skrotzki, J., et al.: A particle-surface-area-based parameterization of immersion freezing on desert dust particles, Journal of the Atmospheric Sciences, 69, 3077–3092, 2012.

Oue, M., Kumjian, M. R., Lu, Y., Verlinde, J., Aydin, K., and Clothiaux, E. E.: Linear depolarization ratios of columnar ice crystals in a deep precipitating system over the Arctic observed by zenith-pointing Ka-band Doppler radar, Journal of Applied Meteorology and Climatology, 54, 1060–1068, 2015.

610 Petäjä, T., O'Connor, E. J., Moisseev, D., Sinclair, V. A., Manninen, A. J., Väänänen, R., von Lerber, A., Thornton, J. A., Nicoll, K., Petersen, W., et al.: BAECC: A field campaign to elucidate the impact of biogenic aerosols on clouds and climate, Bulletin of the American Meteorological Society, 97, 1909–1928, 2016.

Petters, M. and Wright, T.: Revisiting ice nucleation from precipitation samples, Geophysical Research Letters, 42, 8758–8766, 2015.

615 Prill, F., Reinert, D., Rieger, D., Zaengl, G., Schroeter, J., Foerstner, J., Werchner, S., Weimer, M., Ruhnke, R., and Vogel, B.: Working with the ICON Model–Practical exercises for NWP mode and ICON-ART, ICON Model Tutorial, Deutscher Wetterdienst, Offenbach, Germany, 2019.

Proske, U., Bessenbacher, V., Dedekind, Z., Lohmann, U., and Neubauer, D.: How frequent is natural cloud seeding over Switzerland?, Atmospheric Chemistry and Physics Discussions, 2020, 1–33, https://doi.org/10.5194/acp-2020-1145, 2020.

620 Protat, A. and Williams, C. R.: The accuracy of radar estimates of ice terminal fall speed from vertically pointing Doppler radar measurements, Journal of applied meteorology and climatology, 50, 2120–2138, 2011.

Radenz, M., Bühl, J., Seifert, P., Griesche, H., and Engelmann, R.: peakTree: a framework for structure-preserving radar Doppler spectra analysis., Atmospheric Measurement Techniques, 12, 2019.

Rangno, A. L. and Hobbs, P. V.: Ice particles in stratiform clouds in the Arctic and possible mechanisms for the production of high ice

625 concentrations, Journal of Geophysical Research: Atmospheres, 106, 15 065–15 075, 2001.

Reinert, D., Prill, F., Frank, H., Denhard, M., Baldauf, M., Schraff, C., Gebhardt, C., Marsigli, C., and Zängl, G.: DWD Database Reference for the Global and Regional ICON and ICON-EPS Forecasting System, Tech. rep., Tech. rep., Deutscher Wetterdienst, https://www. dwd. de/DWD/forschung/nwv . . . , 2020.

Roberts, P. and Hallett, J.: A laboratory study of the ice nucleating properties of some mineral particulates, Quarterly Journal of the Royal

630 Meteorological Society, 94, 25–34, 1968.

Schneider, J., Höhler, K., Heikkilä, P., Keskinen, J., Bertozzi, B., Bogert, P., Schorr, T., Umo, N. S., Vogel, F., Brasseur, Z., et al.: The seasonal cycle of ice-nucleating particles linked to the abundance of biogenic aerosol in boreal forests, Atmospheric Chemistry and Physics Discussions, pp. 1–18, 2020.

Scott, B. C. and Hobbs, P. V.: A theoretical study of the evolution of mixed-phase cumulus clouds, Journal of the Atmospheric Sciences, 34,

635 812–826, 1977.

Seifert, A.: A revised cloud microphysical parameterization for COSMO-LME, COSMO Newsletter, 7, 25–28, 2008.

Seifert, P., Ansmann, A., Mattis, I., Althausen, D., and Tesche, M.: Lidar-Based Profiling of the Tropospheric Cloud-Ice Distribution to Study the Seeder-Feeder Mechanism and the Role of Saharan Dust as Ice Nuclei, in: Proceedings of the 8th International Symposium on Tropospheric Profiling, edited by Apituley, A., Russchenberg, H. W. J., and Monna, W. A., 2009.

640 Sekelsky, S. M.: Near-field reflectivity and antenna boresight gain corrections for millimeter-wave atmospheric radars, Journal of Atmospheric and Oceanic Technology, 19, 468–477, 2002.

Shupe, M. D., Kollias, P., Matrosov, S. Y., and Schneider, T. L.: Deriving mixed-phase cloud properties from Doppler radar spectra, Journal of Atmospheric and Oceanic Technology, 21, 660–670, 2004.

Shupe, M. D., Walden, V. P., Eloranta, E., Uttal, T., Campbell, J. R., Starkweather, S. M., and Shiobara, M.: Clouds at Arctic atmospheric
645 observatories. Part I: Occurrence and macrophysical properties, Journal of Applied Meteorology and Climatology, 50, 626–644, 2011.

Silber, I., Fridlind, A. M., Verlinde, J., Ackerman, A. S., Cesana, G. V., and Knopf, D. A.: The Prevalence of Precipitation from Polar Supercooled Clouds, Atmospheric Chemistry and Physics Discussions, 2020, 1–32, https://doi.org/10.5194/acp-2020-993, 2020.

Sinclair, V. A., Moisseev, D., and von Lerber, A.: How dual-polarization radar observations can be used to verify model representation of secondary ice, Journal of Geophysical Research: Atmospheres, 121, 10–954, 2016.

650 Spek, A., Unal, C., Moisseev, D., Russchenberg, H., Chandrasekar, V., and Dufournet, Y.: A new technique to categorize and retrieve the microphysical properties of ice particles above the melting layer using radar dual-polarization spectral analysis, Journal of atmospheric and oceanic technology, 25, 482–497, 2008.

Sullivan, S. C., Barthlott, C., Crosier, J., Zhukov, I., Nenes, A., and Hoose, C.: The effect of secondary ice production parameterization on the simulation of a cold frontal rainband, Atmospheric Chemistry and Physics, 18, 16 461–16 480, https://doi.org/10.5194/acp-18-16461-
655 2018, 2018.

Sun, Z. and Shine, K. P.: Studies of the radiative properties of ice and mixed-phase clouds, Quarterly Journal of the Royal Meteorological Society, 120, 111–137, 1994.

Tridon, F. and Battaglia, A.: Dual-frequency radar Doppler spectral retrieval of rain drop size distributions and entangled dynamics variables, Journal of Geophysical Research: Atmospheres, 120, 5585–5601, 2015.

660 Tyynelä, J. and Chandrasekar, V.: Characterizing falling snow using multifrequency dual-polarization measurements, Journal of Geophysical Research: Atmospheres, 119, 8268–8283, 2014.

Tyynelä, J., Leinonen, J., Moisseev, D., and Nousiainen, T.: Radar backscattering from snowflakes: Comparison of fractal, aggregate, and soft spheroid models, Journal of Atmospheric and Oceanic Technology, 28, 1365–1372, 2011.

Vassel, M., Ickes, L., Maturilli, M., and Hoose, C.: Classification of Arctic multilayer clouds using radiosonde and radar data in Svalbard,
665 Atmospheric Chemistry and Physics, 19, 5111–5126, 2019.

Verlinde, J., Rambukkange, M. P., Clothiaux, E. E., McFarquhar, G. M., and Eloranta, E. W.: Arctic multilayered, mixed-phase cloud processes revealed in millimeter-wave cloud radar Doppler spectra, Journal of Geophysical Research: Atmospheres, 118, 13–199, 2013.

Westbrook, C. and Illingworth, A.: The formation of ice in a long-lived supercooled layer cloud, Quarterly Journal of the Royal Meteorological Society, 139, 2209–2221, 2013.

670 Wex, H., Huang, L., Zhang, W., Hung, H., Traversi, R., Becagli, S., Sheesley, R. J., Moffett, C. E., Barrett, T. E., Bossi, R., et al.: Annual variability of ice-nucleating particle concentrations at different Arctic locations, Atmospheric Chemistry and Physics, 19, 5293–5311, 2019.

Wildeman, S., Sterl, S., Sun, C., and Lohse, D.: Fast dynamics of water droplets freezing from the outside in, Physical review letters, 118, 084 101, 2017.

675 Wilson, T. W., Ladino, L. A., Alpert, P. A., Breckels, M. N., Brooks, I. M., Browse, J., Burrows, S. M., Carslaw, K. S., Huffman, J. A., Judd, C., et al.: A marine biogenic source of atmospheric ice-nucleating particles, Nature, 525, 234–238, 2015.

Yang, J., Wang, Z., Heymsfield, A. J., DeMott, P. J., Twohy, C. H., Suski, K. J., and Toohey, D. W.: High ice concentration observed in tropical maritime stratiform mixed-phase clouds with top temperatures warmer than- 8° C, Atmospheric Research, 233, 104 719, 2020.

Young, G., Lachlan-Cope, T., O'Shea, S., Dearden, C., Listowski, C., Bower, K., Choularton, T., and Gallagher, M.: Radiative effects of secondary ice enhancement in coastal Antarctic clouds, Geophysical Research Letters, 46, 2312–2321, 2019.

Zängl, G., Reinert, D., Rípodas, P., and Baldauf, M.: The ICON (ICOsahedral Non-hydrostatic) modelling framework of DWD and MPI-M: Description of the non-hydrostatic dynamical core, Quarterly Journal of the Royal Meteorological Society, 141, 563–579, 2015.

Zawadzki, I., Fabry, F., and Szyrmer, W.: Observations of supercooled water and secondary ice generation by a vertically pointing X-band Doppler radar, Atmospheric Research, 59, 343–359, 2001.

Zhao, X. and Liu, X.: Global Importance of Secondary Ice Production, Geophysical Research Letters, p. e2021GL092581, 2021.

Zhao, X., Liu, X., Phillips, V. T. J., and Patade, S.: Impacts of secondary ice production on Arctic mixed-phase clouds based on ARM observations and CAM6 single-column model simulations, Atmospheric Chemistry and Physics, 21, 5685–5703, https://doi.org/10.5194/acp-21-5685-2021, 2021.

680

685